NJC

Accepted Manuscript

This is an *Accepted Manuscript*, which has been through the Royal Society of Chemistry peer review process and has been accepted for publication.

Accepted Manuscripts are published online shortly after acceptance, before technical editing, formatting and proof reading. Using this free service, authors can make their results available to the community, in citable form, before we publish the edited article. We will replace this *Accepted Manuscript* with the edited and formatted *Advance Article* as soon as it is available.

You can find more information about *Accepted Manuscripts* in the Information for Authors.

Please note that technical editing may introduce minor changes to the text and/or graphics, which may alter content. The journal's standard Terms & Conditions and the Ethical guidelines still apply. In no event shall the Royal Society of Chemistry be held responsible for any errors or omissions in this *Accepted Manuscript* or any consequences arising from the use of any information it contains.

ROYAL SOCIETY OF CHEMISTRY

www.rsc.org/njc

The New journal of Chemistry

ARTICLE

New Journal of Chemistry

Impact of extreme downsizing of *BEA-type zeolite crystals on n-hexadecane hydroisomerization

Received 00th January 20xx,
Accepted 00th January 20xx

DOI: 10.1039/x0xx00000x

www.rsc.org/

Amir Astafan[a,b], Yannick Pouilloux[a], Joël Patarin[b], Nicolas Bats[c], Christophe Bouchy[c], T. Jean Daou[b]†, Ludovic Pinard[a]††

Abstract : A series of *BEA-type zeolites with a crystal sizes ranging from few nanometers to micrometer were synthesized. These materials were then transformed into bifunctional catalysts by platinum loading and tested in n-hexadecane isomerization. Pt/H-*BEA catalysts behavior depends on lot of parameters such as the balance between the platinum and acid functions, the metal particle size and the zeolite crystal size. In order to design an "ideal" bifunctional catalyst, the balance between metal and acid sites must be enough to avoid the cracking of isomer products at low conversion, the metal must be well dispersed in order to inhibit the hydrogenolysis side reactions, and the crystal size must be as small as possible to maximize the isomers yield. But, the extreme decrease of zeolite crystal thickness to few zeolite unit cells lowers the turnover frequency of acid sites, and favored the metal sintering.

1. Introduction

The rational design of bifunctional redox-acid refining catalysts requires the definition of the parameters governing their behavior and the knowledge of their quantitative effect. This is what has been successfully achieved with isomerization dewaxing Pt-H-zeolite catalysts [1-4]. n-Alkane hydroisomerization involves 7 successive steps: 3 chemical ones, dehydro-hydrogenation on the Pt sites and alkene skeletal isomerization on the protonic acid sites (H^+) and 4 diffusion ones in gas phase (alkanes) and along the zeolite micropores (alkenes) from the Pt to the H^+ sites and vice versa [1]. When considering this scheme, it appears that the behavior of Pt/zeolite catalysts is function of the balance between the platinum (Pt) and acid (H^+) functions and of the characteristics of zeolite micropores [2-4].

The catalyst activities and especially the reaction scheme depend strongly on the zeolite pore structure: monobranched and multibranched isomers are the main products on Pt/H-*BEA, while cracking is the main reaction observed on Pt/H-MCM-22 and Pt/H-ZSM-5 with long-chain paraffin [5]. This can be explained by the diffusion inside the zeolite porosities: rapid diffusion inside the large channels of the H-*BEA zeolite, blocking of the reaction intermediates inside the porosity of H-MCM-22 and H-ZSM-5 yielding extensive cracking. Pt/H-ZSM-22, a monodimensional medium pore zeolite shows an unexpected very high selectivity to monobranched isomers [6-8]. The acid sites located at the pore entrance are only accessible to long chain n-alkene intermediates, which makes the Pt/H-ZSM-22 catalyst very selective for the formation of monobranched isomers. The fast initial blockage of the channels by carbonaceous compounds supports the proposal of a pore mouth mechanism for n-alkene isomerization [9]. The small number of accessible H^+ sites in pore mouth which accounts for the relatively low activity contributes also in increasing the selectivity.

Regardless of zeolite structure, the sine qua non condition to design an "ideal" bifunctional catalyst is that acidic and metallic functions must absolutely be "well" balanced. The first tentative of quantification was made in n-C_7 and n-C_{10} hydroisomerization on a series of Pt/H-FAU catalysts [10]. A positive effect of the C_{Pt}/C_A ratio between the concentrations of accessible Pt (C_{Pt}) and (protonic) acid sites (C_A), chosen for quantifying the Pt/H^+ balance, is observed. The optimal stability and selectivity to isomers are however obtained at higher C_{Pt}/C_A values than the optimal activity per acid site (turnover frequency, TOF) [11]. This shows that "ideal" bifunctional catalysis requires not only that

[a] Institut de Chimie des Milieux et Matériaux de Poitiers, UMR 7285 CNRS, 4 Rue Michel Brunet, Bâtiment B27, 86073 Poitiers Cedex9 France.
[b] Université de Strasbourg, Université de Haute Alsace, Equipe Matériaux à Porosité Contrôlée (MPC), Institut de Science des Matériaux de Mulhouse (IS2M), UMR CNRS 7361, ENSCMu, 3 bis rue Alfred Werner, 68093 Mulhouse Cedex, France..
[c] Energies nouvelles, Rond-point de l'échangeur de Solaize, BP 3, 69360 Solaize, France.

† Email: jean.daou@uha.fr, Tel: +33 (0) 389 336 739, Fax: +33 (0) 389 336 885.
†† Email: ludovic.pinard@univ-poitiers.fr, Tel: +33 (0) 549 453 905, Fax: +33 (0) 549 453 774.

Electronic Supplementary Information (ESI) available: See DOI: 10.1039/x0xx00000x

hydroisomerization is kinetically limited by the acid steps but that the olefinic intermediates undergoes only one skeletal rearrangement or cracking step during their diffusion between two Pt sites [1,2]. This led us to propose recently the average number of acid steps (n_{as}) involved in the apparent formation of products from one reactant molecule as an additional determining parameter of the bifunctional process [12,13]. n_{as} depends on both the intimacy between Pt and H^+ sites (actually on n_{H+} between two Pt sites) and on the H^+ efficiency under the operating conditions, which precludes its estimation from the physicochemical catalyst characteristics. A simple method was thus developed to estimate n_{as} from the product composition. n-C_{16} hydroisomerization over 3 series of Pt-H-*BEA samples based on the same zeolite but with large differences in Pt-H^+ proximity confirms that the catalytic behavior is determined by C_{Pt}/C_{H+} (C_{H+} was determined by pyridine followed by FTIR) and n_{as} only [12, 13]. Indeed, a unique curve is obtained by plotting $TOF_{corrected} = TOF.n_{as}$, expressed in mole of olefinic intermediates transformed per mole of H^+ and per hour versus C_{Pt}/C_{H}^+. With all the samples, n_{as} values >1 are found, which is related to the large *BEA nanocrystal aggregates.

To limit to 1 the number of acid sites encountered by intermediates (alkenes), it appears as evidence that beta crystal must be limited to few unit cells. Owing to the development of zeolite synthesis using gemini-type quaternary ammonium surfactant, ultrathin Beta zeolite of a few nm, defined as nanosponge by Ryoo and coworkers, can be now synthetized [14-17]. Hence, a Pt/nanosponge H-*BEA catalyst appears to gather all conditions to be an "ideal" bifunctional catalyst.

The purpose of the present work is to evaluate the impact of the extreme downsizing of beta zeolite on the hydroisomerization reaction. To address these points, several beta zeolites were synthesized with different particle sizes and morphologies: four materials constituted of large crystals ranging from 0.2 to 10 µm and two hierarchical porous zeolites with a mesoporous network created either by the aggregation of nanometer-sized crystals or by the use of a particular organic surfactant (yielding into nanosponge zeolite). The catalytic performances of these Pt-supporting zeolites for hydroisomerization are investigated using n-hexadecane as substrate, which is very sensitive to cracking.

2. Experimental section

2.1. Synthesis of bifunctional catalysts

Table 1 resumes the molar composition of formulation gels and the thermal conditions used to synthesize *BEA-type zeolites. The synthesis protocols, available in the open literature [14-19], are detailed in the supporting information (SI). The protonic form of zeolites was obtained by double ion-exchange of the calcined sample with a 1M NH_4NO_3 solution (liquid/solid ratio: 20 mL/g) at 80 °C for 1 h and calcination in a static oven at 550 °C for 5 h.

The bifunctional catalysts are obtained by ion exchange (IE) of acidic zeolite using an aqueous solution of platinum salt. The concentrations of platinum salt in the exchange solution are determined in order to achieve a Pt content of 2 wt % on all zeolites and 5 wt % only on the MC(17) sample. The proportions of zeolite and metal salt in solution are calculated by assuming a total exchange between platinum precursor and zeolite protons. For example, 1.0 g of zeolite is added to a 50 mL aqueous solution containing 0.0397 g of $Pt(NH_3)_4(NO_3)_2$ salt (98 %, Sigma-Aldrich). The exchanging solution contained n_{NH4}^+/n_{Pt} molar ratio of 100 achieved by addition of NH_4NO_3 aqueous solution (1 M). IE is performed during 24 h under stirring at room temperature. Then the exchanged zeolite is filtered, dried at 90 °C overnight and calcined under air flow (150 mL min^{-1}) at 450 °C for 5 h (ramp heating 2 °C min^{-1}).

Table 1. Molar composition of the starting synthesis gels and thermal conditions for the preparation of micron-sized (MC), submicron-sized (SC), nanometer sized (NC) crystals and nanosponge (NS)*BEA-type zeolites.

	catalyst	MC(23)	MC(17)	SC(17)	SC(13)	NC(23)	NS(22)
Reagents	Si	TEOS [d]	TEOS [d]	TEOS [d]	Aerosil 130	SiO_2 [a]	TEOS [d]
	Al	$Al_{(s)}$	$Al_{(s)}$	$Al_{(s)}$	$NaAlO_2$	$Al(O\text{-}iPr)_3$	$NaAlO_2$
Gel composition in molar ratio	HF	0.573	0.700	0.680	-	-	-
	Na_2O	-	-	-	0.020	0.014	0.220
	$(TEA)_2O$ [b]	0.226	0.226	0.340	0.140	0.180	-
	$N_{4\text{-phe}}$ [c]	-	-	-	-	-	0.050
	Al_2O_3	0.016	0.040	0.070	0.016	0.020	0.025
	SiO_2	1	1	1	1	1	1
	$(Et)_2O$	-	-	-	-	-	4.00
	H_2O	7.03	8.00	7.14	15.75	11.80	71.00
Temp	(° C)	170	170	170	150	95	140
Time	(days)	14	8	14	16	9	4
Ref		[18]	[18]	[19]		[20]	[14-17]

[a] Ludox AS(40) 40 % in water lyophilized for 5 days; [b] TEA : $(CH_3\text{-}CH_2)N$-; [c] $N_{4\text{-Phe}}$: $C_{22}H_{45}N^+(CH_3)_2C_6H_{12}N^+(CH_3)_3(Br)^-$; [d] TEOS: $Si(OCH_2CH_3)_4$; Et : $CH_3\text{-}CH_2\text{-}OH$

2.2. Physicochemical properties

Characterization methods were previously described in ref. [21]. The structural characterization of the zeolites was carried out by X-ray powder diffraction (XRD) on a PANalytical MPD X'Pert Pro diffractometer operating with Cu Kα radiation (λ = 0.15418 nm) and equipped with an X'Celerator real-time multiple strip detector (active length = 2.122 ° 2θ). Morphology, homogeneity and particle sizes were determined with a scanning electron microscope (SEM) (Philips XL30 FEG). Nitrogen adsorption and desorption measurements were carried out at –196 °C on a Micromeritics ASAP 2420 apparatus. Prior to analysis, the samples were pretreated at 300 °C under vacuum for 15 h. The specific area (S_{BET}) was calculated according to the BET method using the following areas $2.10^{-4} < p/p_0 \leq 8.10^{-2}$ and $4.10^{-3} < p/p_0 \leq 12.10^{-2}$ for microcrystals and hierarchical materials (nanosponges, nanocrystals) respectively. The microporous volumes (V_{micro}) were calculated using the t-plot method. The pore size distributions were determined using Density Functional Theory (DFT) model applied on the adsorption branch. The total pore volume was calculated at $p/p_0 = 0.9$. Both mesopore volume (V_{meso}) and catalyst external surface (S_{ext}) were determined by the difference between the total pore volume and the micropore volume.

Silicon to aluminun molar ratio were determined by X-Ray Fluorescence spectrometry (Philips, Magic X), whereas the zeolite framework aluminun (Al^{IV}) content was estimated from infrared spectroscopy measurement on a FT-IR Magna 550 Nicolet spectrometer. The position of the zeolite structure bands (450-1250 cm^{-1}) allowed calculating framework aluminun from the correlation given in literature [22]. ^{27}Al magic angle spinning nuclear magnetic resonance (^{27}Al MAS NMR) spectra were recorded at 104.28 MHz on a Bruker advance II 400 MHz spectrometer using a spinning rate of 12 kHz, a pulse length of 0.42 μs and a recycle time of 0.58 s.

The X-Ray photoelectron spectra (XPS) were measured with a Kratos Axis Ultra DLD spectrometer. The photoelectron spectra were measured using a monochromatic Al Kα source (1 486.6 eV) operating at 150 W (10 mA, 15 kV). The base pressure .in the analysis chamber during measurements was 9×10^{-8} Pa. The charge neutraliser system was operated for all analysis to compensate for the buildup of positive charge due to insulating samples. Spectra were recorded with constant pass energy of 160 eV. The binding energies were referenced to the Si2p core level (103 eV). The composition and chemical surrounding of the sample surface was investigated on the basis of the areas and binding energies of Al2p, Si2p and O1s photoelectron peaks. The fitting of high resolution spectra was provided through the CasaXPS software.

The zeolite acidity was quantified by infrared spectroscopy by using two basic probe molecules: ammonia and pyridine [23]. In some experiments, an excess of pyridine or ammonia was sorbed at 50 °C (in the case of ammonia) or 150 °C in the case of pyridine, and after 30 min contact with the sample, physically base were evacuated at the same temperatures. The platinum content of bifunctional catalysts was determined by inductively coupled plasma-atomic emission spectroscopy (ICP-AES). The number of accessible platinum atoms (n_{Pt}) of the catalysts was estimated by CO adsorption at room temperature, followed by infrared spectroscopy. The platinum particle size was visualized by transmission electron microscopy (TEM) using a Jeol microscope model ARM-200F, under an acceleration voltage of 200 kV.

2.3 n-C_{16} hydroisomerization

The transformation of n-C_{16} (Aldrich, 99.9 %) was carried out in a fixed bed stainless steel reactor under a total pressure of 3 MPa and a H_2/n-C_{16} molar ratio of 20. Two methods were used to change the conversion i) the temperature (220-250 °C) was increased by stepwise at constant space time, ii) the n-C_{16} weight hourly space velocity (WHSV) was changed in the range of 2 to 100 h^{-1} at fixed temperature (220 °C).

To avoid condensation during the products analysis, n-C_{16} was diluted with n-hexane (n-C_6/n-C_{16} ratio=9), which is inert under the operation conditions. The catalyst bed was composed from 0.1 to 1 g of catalyst with 0.2-0.4 mm particle size and mixed with carborumdum (ø = 0.25 mm). Before reaction, all catalysts were reduced under a hydrogen flow at 450 °C for 6 h. The reaction products were analyzed on-line through GC on 50 m CPSil-5 capillary column from Chrompack, with hydrogen as carrier gas (13 psi) and a FID detector.

3. Results and discussion

3.1. Morphology and textural properties of the *BEA zeolites

Six samples of *BEA-type zeolite with different crystal sizes (thicknesses) are obtained as described in supporting information (SI). The samples are designed by MC(17), MC(23), SC(17), SC(13) NC(23) and NS(22). Capital letters refer to the crystal size, i.e. MC, SC and NC for micrometer, sub-micrometer and nanometer-sized crystal, respectively and NS for nanosponge. Number in bracket corresponds to Si/Al molar ratio of the framework. The structural, textural and acidic properties of each sample are characterized by XRD, N_2 adsorption, SEM, TEM, XRF, XPS, and adsorption of pyridine followed by FTIR. Their main features are summarized in table 2.

Table 2. Selected characteristics of micron-sized (MC), sub-micron-sized (SC), nanometer-sized (NC) crystals and nanosponge (NS) *BEA-type zeolites.

Zeolite	Unity	MC(17)	MC(23)	SC(17)	SC(13)	NC(23)	NS(22)
Crystal size	µm	6-10	6-10	0.3-1.5 [a]	0.2-1 [a]	0.04 [b]	0.002-0.004 [c]
S_{BET} [d]	$m^2\ g^{-1}$	588	626	680	709	726	977
S_{ext} [e]	$m^2.g^{-1}$	13	33	160	170	223	185
V_{micro} [f]	$cm^3\ g^{-1}$	0.22	0.23	0.25	0.25	0.24	0.3 [g]
V_{meso} [h]	$cm^3\ g^{-1}$	0.02	0.05	0.12	0.29	0.71	0.74
Si/Al_{global} [i]	molar	15	14	9	10	15	17
Si/Al_{fram} [j]	molar	17	23 (20)	17	13	23 (21)	22 (23)
Si/Al_{surf} [k]	molar	16	35	11	12	19	22
EFAL [l]	atom per cell	0.5	1.7	3.1	1.4	1.4	0.8
$[H^+]_{th}$	$\mu mol\ g^{-1}$	925	695	926	1115	650	690
$[NH_4^+]^m$	$\mu mol\ g^{-1}$	920	644	770	1124	637	295
$[PyH^+]^n$	$\mu mol\ g^{-1}$	920	620	566	961	443	130
$[PyL]^n$	$\mu mol\ g^{-1}$	215	107	490	186	336	176

[a] apparent average size determined by using SEM and [b]TEM (Fig. 1), respectively ; [c] Nano-sized zeolite crystals separated by mesoporous channels of approximately 4 nm; [d] Specific surface area measured by BET; [e,f]External surface and micropore volume calculated by using t-plot method, respectively; [g] Part of the micropore volume corresponds to interparticular porosity (pore diameter close to 0.15 nm); [h]Mesopore volume =V_{total}-V_{micro} (V_{total}: determined from the adsorbed volume at p/p_0=0.99);i Measured by XRF; [j]Drawn from TOT band at 1080-1200 cm^{-1} using the correlation given in ref [22] and in brackets from ^{27}Al MAS NNR; [k]Measured by XPS, [l]Extra-framework aluminun calculated from [i] and [j; m]Measured by ammonia absorbed on Brønsted (NH_4^+) acid sites, after evacuation at 50 °C. [n]Measured by pyridine adsorbed on Brønsted (PyH^+) and Lewis (PyL) acid sites, respectively, after evacuation at 150 °C.

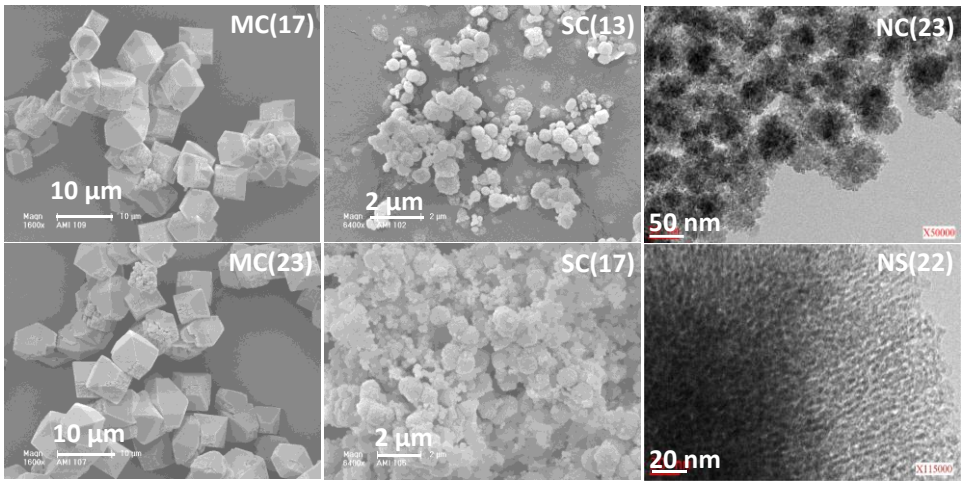

Figure 1. Scanning electron microscopy images of MC(17), MC(23), SC(13) and SC17) samples and Transmission electron microscopy images of nanometer-sized crystal NC(23) and nanosponge NS(22) *BEA-type zeolites.

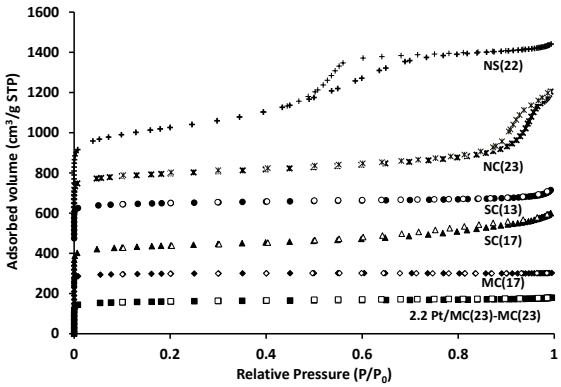

Figure 2. N_2 adsorption (solid symbol) and desorption (open symbol) isotherms at -196 °C of *BEA-type zeolite samples. Isotherms are vertically offset by equal intervals (+100).

The crystalline structure of *BEA-type zeolite is confirmed on all samples by XRD patterns exhibiting Bragg diffraction peaks. No broad peaks attributable to amorphous impurities are detected as shown on the figure SI1. The crystal sizes are estimated from SEM images for micrometer and sub-micrometer crystals and TEM images for the NC(23) and NS(22) samples (Fig. 1).

The MC samples, synthesized in fluorine medium at 170 °C, exhibited the characteristics truncated bipyramidal shape of beta zeolite with a crystal size ranging from 6 to 10 µm. The increase of the percentage of tetraethyl ammonium hydroxide and aluminum in the starting synthesis gel (Table 1) led to great morphological changes of beta material. Indeed, the SEM image of the SC(17) sample is very different from that of the MC(17) sample. An aggregation of crystals with a wide distribution of diameters ranging from 0.3 to 1.5 µm can be observed for SC(17) sample. The SC(13) sample, synthesized in alkaline medium at 150 °C, is constituted of crystals with a smaller diameter (0.2-1 µm). The TEM image of the NC(23) sample exhibits an aggregation of nanometer-sized crystals (ø = 40 nm), whereas that of the NS(22) sample, synthesized by using a poly-quaternary ammonium surfactant, reveals a nanosponge-like morphology. These nanosponges are constituted by randomly aggregated nanoparticles delimited by ordered mesoporous channels. Moreover, the presence of nano-sized beta crystals with a size going from 2 to 4 nm separated by channels of approximately 4 nm in diameter are observed. Note that no mesopores are observed by SEM in the bulk of the two micrometer-sized zeolite samples.

This observation is also confirmed by the N_2 adsorption-desorption isotherms performed on the micrometer crystals. A strong uptake of N_2 at low relative pressure and a plateau at high relative pressure, which is typical for microporous materials (type I according to IUPAC classification [24]) is observed for micrometer crystals as shown in figure 2. Application of the BET model and t-plot method confirms that the majority of the surface area (S_{BET} 590-630 $m^2\ g^{-1}$) is due to the presence of micropores, whereas the contribution of mesoporosity is almost null. The micropore volume of 0.23 g. cm^{-3} (Table 2) is typical of a *BEA zeolite. It is independent on the zeolite crystal size as already observed in the open litterature. [25] The higher micropore volume on the NS(22) sample probably arises from the formation of supermicropores (pore diameter close to 15 nm) in addition to BEA zeolite micropores. On the sub-micrometer-sized samples, an upwards deviation of the plateau for relative pressure near 1 is observed pointing out an increase of the mesoporosity (0.12-0.29 $cm^3\ g^{-1}$) and external surface (160-170 $m^2.\ g^{-1}$). The nanometer-sized materials NC(23) present isotherms of Ib and IV types. The step at high p/p_0 relative pressures (0.75-0.95) indicates the presence of intergrain mesoporosity which is due to the agglomeration of the zeolite nanoparticles. The isotherms of nanosponge zeolite NS(22) are also of Ib and IV types as shown in figure 2. The mesopores revealed by the step in the p/p_0 = 0.3-0.80 range are generated by the use of the organic surfactant and are characterized by a high adsorbed volume (mesoporous volume) as shown in Table 2. The mesopore size distribution is centered between 3 to 4 nm.

3.2. Acidic properties of the *BEA zeolites

For all materials, the global Si/Al molar ratio, measured by XRF (Si/Al_{global} =9-17) was lower than the Si/Al framework ratio determined from TOT bands (Si/Al_{fram} = 13-23). The values of the Si/Al_{fram} molar ratios were confirmed on three samples by ^{27}Al MAS NNR measurements (values in brackets in table 2). Regardless of the synthesis protocol, a significant fraction of the Al atoms initially present (ca. 20 to 30 %) in the gel composition (Table 1) did not end up in the framework of beta zeolite (Table 2). This difference suggests the presence of extra framework aluminun species (EFAL), which were estimated between 0.5 and 3.1 per zeolite unit cell (Table 2). No correlation exists between the amount of EFAL and the concentration of Lewis acid sites measured by adsorption of pyridine followed by FTIR.

The values of Si/Al_{surf} determined by XPS were quasi identical to the Si/Al_{fram} on the MC(17), SC(13), NC(23) and NS(22) samples (Table 2). The distribution of aluminum between the surface and the bulk crystal on these materials is homogeneous, in contrary of the MC(23) and SC(17) samples. The first presented a deficiency of Al in the surface zone compared to the bulk phase while the surface of SC(17) was enriched in Al.

The concentrations of Brønsted acid sites determined by ammonia adsorption (Fig. SI.2) were comparable with the values $[H^+]_{th}$ calculated from the chemical composition of zeolites, except for two samples: SC(17) and NS(22) (Table 2), the difference are ca. 15% and ca. 40%, respectively. On the first, the slight discrepancy probably arises from a partial blockage of access of acid sites due to the presence of lot of EFAL; particularly high in this sample (more than 3 atoms per unit cell). This partial blockage was confirmed by using a larger probe, (i.e. pyridine): the difference between $[PyH^+]$ and $[H^+]_{th}$ increase up to 40%. On the NS(22)sample, the high gap between $[H+]_{th}$ and $[NH_4^+]$ is not due to presence of EFAL (only 0.8 atom per unit cell), but it could be related to the decrease of the strength of the acid sites arising from the extreme decrease of the *BEA crystal size. Pyridine and ammonia are sensitive to sites of differing strength. In the case of the micrometer-sized zeolites, all protonic sites were probed by pyridine. But the $[PyH^+]/[H^+]_{th}$ ratio, contrariwise with ammonia, had a tendency to decrease with the crystal downsizing; on the nanometer-sized zeolite only ca. 70 % of acid sites were able to retain pyridine at 150 °C, this percentage fell to ca. 20 on the nanosponge zeolite. The major part of aluminum present in the framework of the nanosponge zeolite generates very weak acid sites. The strength of acid site decreases with the zeolite crystal size, and dramatically when the zeolite crystal thickness is only of few unit cells as confirmed by ammonia TPD (figure SI3).

3.3. Properties of the bifunctional catalysts

As shown in table 3, the platinum loading by ion exchanges is total on the MC and SC samples and surprisingly partial on the hierarchical nanometer-sized zeolites. Consequently, the platinum content were ca. 2 wt % and 5 wt % on the large crystals, slightly lower on the NC sample (1.8 wt %) and only 1.4 wt % on the nanosponge zeolite. The decrease of the efficiency in IE could be due (by assuming that the ionic exchange occurs only with strong acid site) to the increase of molar ratio between the concentrations of platinum salt and Brønsted acid sites. On the large crystals it was lower than ca 1/6 whereas on the NS sample it was close to the unity.

The dispersion (D), defined as the amount of platinum atoms at the surface by the total number of platinum atoms is measured by CO chemisorption at 25 °C. The Pt dispersion was rather low and similar (20-30 %) on the crystal catalysts (MC, SC and NC). On the nanosponge catalyst, D is even lower (10 %), in spite to a lower platinum content. The Pt particle aggregation that occurs during the reduction of $Pt(NH_3)_4^{2+}$ seems favored by the extreme zeolite downsizing. The equation of d_{chem}(nm) = 1.13/D is conventionally used to calculate the Pt particle diameter [26]. The Pt particle average sizes ranged between 4 to 6 nm on the crystal zeolites (MC, SC and NC) and is ca. 11 nm on the NS sample. In the case of the nanometer catalysts (NS and NC), Pt particle diameters calculated using this equation are in very good agreement with those determined by TEM (Fig. 3). Therefore, most of the platinum particles were located on the external surface. In the case of 2.2Pt/MC(23), the Pt particle diameter measured by TEM is ca 5 times higher than that calculated from dispersion. This observation can only be explained by a bimodal distribution of metal particles i.e. one part located in the external surface (d_{Pt}= 27 nm), and the other part, undetectable by TEM, inside the zeolite. The XRD patterns of 2.2Pt/MC(23) catalysts compared to MC(23) showed 2 additional peaks due to the large platinum particle (Fig. SI.1). It is possible to estimate their percentage by assuming that the metal particle size is equal to the *BEA pore dimension (0.66 x 0.67 nm); ¾ of Pt particles were inside the zeolite pore. The micrometer-sized crystal seems to avoid particle sintering during the platinum precursor reduction whereas the ultra-thin thickness of nanosponge favors the platinum migration to the external surface. The conditions of the reduction of platinum should be very soft in order to limit the aggregation of metal on the external surface of ultrathin zeolite crystal.

Table 3. Physicochemical characteristics of the bifunctional catalysts: Pt dispersion (D) estimated by CO chemisorption, concentration of accessible Pt atoms (C_{Pt}), average diameter of platinum particles (d_{Pt}) and balance between hydrogenating and acid functions (C_{Pt}/[PyH+]

Catalyst	Pt exchange (%)	D [a] (%)	d_{chem} [b] (nm)	d_{Pt} [c] (nm)	C_{Pt} (µmol g^{-1})	$C_{pt}/[PyH^+]$
2.0Pt/MC(17)	100	24	4.7	-	24.6	0.027
5.0Pt/MC(17)	100	20	5.7	-	51.3	0.057
2.2Pt/MC(23)	100	20	5.7	27	22.6	0.054
2.0Pt/SC(13)	100	23	4.9	-	23.5	0.024
2.1Pt/SC(17)	100	28	4.0	-	30.1	0.053
1.8Pt/NC(23)	90	30	3.8	4.3	27.6	0.063
1.4Pt/NS(22)	70	10	11.3	9.2	7.2	0.055

[a]Measured by CO chemisorption at 25 °C, [b]mean particle diameter calculated according to equation d (nm) = 1.13/D, where D is the metal dispersion, c mean particle diameter determined by counting a minimum of 200 particles.

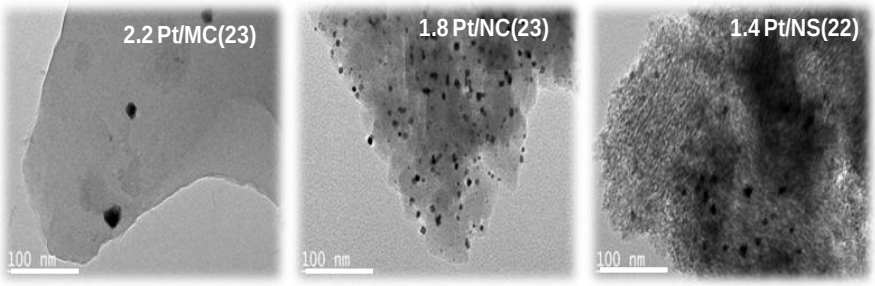

Figure 3. Representative transmission electron microscopy images of 2.2Pt/MC(23), 1.8Pt/NC(23) and 1.4Pt/NS(22) catalysts.

Table 4. Activities values measured at 220 °C per gram of catalyst and per acid sites (TOF, and of the initial ratios between cracking and isomerization products $(C/I)_0$ and between multibranched and monobranched isomers $(B/M)_0$. n_{as}, number of acid steps involved in the apparent transformation of one n-C_{16} molecule.

Catalyst	Activity at 220°C [a] (mol_{nC16} g_{cat}^{-1} h^{-1})	TOF [b] (mol_{nC16} mol_{H+} h^{-1})	$(B/M)_0$	$(C/I)_0$	n_{as} [c]
2.0Pt/MC(17)	-	-	0.90	0.5	2.47
5.0Pt/MC(17)	0.0029	3.2	0.51	0.06	1.64
2.2Pt/MC(23)	0.0043	10.2	0.35	0.04	1.48
2.0Pt/SC(13)	0.0073	7.6	1.1	0.8	2.76
2.1Pt/SC(17)	-	-	0.40	0.02	1.48
1.8Pt/NC(23)	0.0035	8.0	0.10	0.03	1.20
1.4Pt/NS(22)	0.0003	2.6	0.09	0.00	1.08

[a] Measured at conversion <20 % , [b] Calculated by using the BAS concentration reported in Table 3 and in bracket by a concentration estimated to be 530 µmol g^{-1} , [c] Number of acid steps involved in the apparent transformation of one molecule of n-C_{16} [12-13]

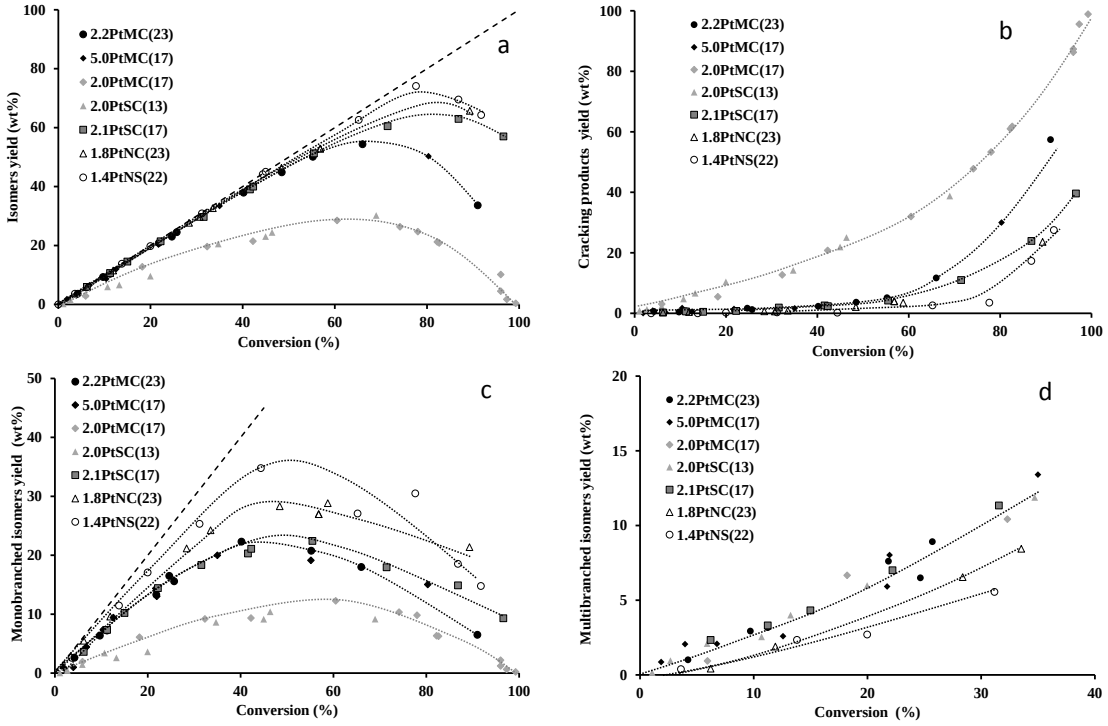

Figure 4. Yields into: isomers (a) cracking products (b), monobranched (c) and multibranched (d) isomers as a function of conversion on a series of bifunctional catalysts. Catalytic tests carried out by changing temperature (220-250 °C) and WHSV (2-100 h^{-1})

The concentration of Brønsted acid sites (BAS) on the bifonctional catalyst (2.2Pt/MC23), should be lower than that on the corresponding micrometer-sized zeolite (MC(23)). By assuming that one Pt atom substitutes one protonic site, the concentration of BAS on platinum catalyst should be around of 530 µmol g^{-1}, against 620 on the MC(23) sample; actually it is 420 µmol g^{-1}

Table 3 shows that for all the catalysts, the concentration of the accessible Pt sites (C_{Pt}) is much lower than the density of protonic sites measured by pyridine adsorption ([PyH^+], Table 2). As a consequence, the values of the C_{Pt}/[PyH^+] ratio, which was chosen as representative of the balance between the hydrogenating function and the acid function, were very low, ranging between 0.027 and 0.063.

3.4. n-C_{16} hydroisomerization over Pt/*BEA zeolites

3.4.1. Activities. Under the operating conditions, all the catalysts exhibited a very stable activity for n-C_{16} transformation, which indicated that the amount of platinum was enough to avoid the transformation of olefinic intermediates into coke. The activities measured at 220 °C and at a conversion lower than 20 % are reported in Table 4. The

values ranged between 0.0003 and 0.073 mol_{nC16} g_{cat} h^{-1}. Therefore, the rate limiting reactions are not occurring on the hydrogenating function (platinum) but on the acidic functions. Then, it is logical to assume in first approximation that the activity is proportional to the concentration of accessible acid sites measured on the protonic zeolites (i.e. [PyH^+]). The turnover frequency (TOF), expressed as mole of n-hexadecane converted per mole of Brønsted acid site is similar on 2.2Pt/MC(23), 2.0Pt/SC(13) and 1.8Pt/NC(23) (7.6-10.2 mol_{nC16} $mol_{H+}.h^{-1}$). The nearly constant value of TOF for different crystal sizes strongly suggests that there is no diffusion limitation under the present operating conditions of n-hexanedecane isomerization. The lower activity in 5.0 Pt/MC(17, could be attributed to an overvaluation of BAS concentration(see part 3.3). However, a lower acid strength for a lower activity would rather the low TOF of 1.4 Pt/NS(22). This interpretation also adopted in the literature for the low activity of Pt/ZSM-5 in n-decane isomerization and hydrocracking when 2 nm thin crystals are used instead of bulkier ones (27). A more direct proof of the decrease of acidity in ultra down sized crystal is obtained from reaction catalyzed by acid site only such as methanol to hydrocarbons, Claisen-Schmidt condensation, etc), Ryoo and coll. [28] have shown that the extreme downsizing zeolite crystal to few unit zeolite cells impacted the "strength" or rather the activity of Brønsted acid site in spite of a better accessibility. These results confirm the conclusion established in part 3.2, i.e. the strength of Brønsted acid sites on the NS(22) sample are relatively weak.

3.4.2. Selectivity's and reaction schemes Monobranched isomers (M), bi-(multi)branched isomers (B) and cracking products (C) were formed over all bifunctional catalysts. M are, mainly, methylpentadecanes. Ethyl-branched isomers are formed in very small amounts and propylbranched isomers were not observed. While B are not formally identified. With all bifunctional catalysts, cracking products (C) were mainly C_3-C_{13} linear and branched products. For most of the present catalysts, the absence of methane and the very low amount of ethane in the C products suggest that hydrogenolysis over platinum sites can be neglected. In contrast, the significant hydrogenolysis activity of the bifunctional nanosponge is attributed to the particularly large Pt particles observed by TEM in this system**.** For example, the yield into cracking products by hydrogenolysis is up to 3 % at 20 % n-C_{16} conversion (SI.3). So, in order to facilitate the comparison between all catalysts, the yields into M, B and C obtained on 1.4Pt/NS(22) are corrected by suppressing the part due to the hydrogenolysis of n-C_{16} (yields into methane and ethane). The product distribution only depends on the catalyst and on the degree of n-C_{16} conversion. Among other properties in hydroconversion, the production of only one isomer independently of the conversion is highly regarded particularly in the absence of shape selectivity as in the present case. According to the literature, it occurs when the operating conditions affect identically both isomerization and hydrogenolysis [28,29] Fig.4 shows the yields in isomers (M+B), M, B and C are plotted vs. n-C_{16} conversion obtained at different temperatures (220-250 °C) and WHSV (2-100 h^{-1}). The dotted line corresponds to a totally selective formation of isomers from n-hexadecane. Initial values (obtained by extrapolation of the curves at zero conversion) of the $(B/M)_0$ and $(C/I)_0$ ratios are reported in Table 4. On the higher acidic bifunctional catalysts, i.e. 2.0Pt/MC(17) and 2.0Pt/SC(13), isomers yields deviate at low conversion of the dotted line and M, B and C products are all apparent primary reaction products (Fig. 4).

The B/M and C/I initial ratios are ca. 1 and higher than 0.5, respectively (Table 4). This parallel scheme of n-C_{16} transformation is typical of an "unbalanced" bifunctional

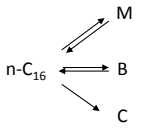

catalyst (Scheme 1).

Scheme 1

However, B isomers and C cracking products cannot be formed directly from n-C_{16} but only from M isomers. This means that the olefinic intermediates formed on Pt encountered several acidic sites inside the zeolite during the diffusion between two hydrogenating sites, yielding M isomers, then B isomers, and finally C products. The average number of active acid sites (n_{as}) encountered by the olefinic intermediates during their diffusion between two Pt sites is equal to the number of acid rearrangement or cracking steps involved in the transformation of one reactant molecule. A method recently proposed by Guisnet and coworkers [13] to estimate nas from the product distribution extrapolated at zero conversion: 2.5 to 2.8 active acid sites (Table 4) are encountered by the olefinic intermediates during their diffusion between two Pt sites, and consequently the maximum yield into isomers is low (only 30 % at 70 % conversion, Fig.4a). Two evident ways exist to rebalance a bifunctional catalyst either by simply increasing the platinum content or by decreasing the Si/Al framework. On 5.0Pt/MC(17), 2.2Pt/MC(23) and 2.1Pt/SC(17), the balance between acidic and metallic functions are now higher than 0.03. At low conversion, the experimental yield in isomers follows the dotted line (Fig. 4.a) and the initial C/I ratios are almost null (Table 4). Regardless of the way used to balance the bifunctional catalysts, isomers are now primary products (C products resulted from a secondary transformation of isomers). Moreover, as on the three catalysts the B/M initial ratios are no null (they are between 0.35 and 0.5 (Table 4)), B products still appeared as a primary product. The rebalance of the two active functions led to a change in the scheme of n-C_{16}

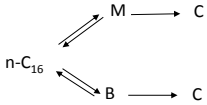

transformation, initially parallel (scheme 1) is become partially successive (scheme 2).

Scheme 2:

But, the maximum yield into isomers depended on the zeolite crystal size: on the two micrometer-sized (MC) and sub-micrometer (SC) catalysts, they were 55 and 66 % at n-C_{16} conversions of 66 and 77 %, respectively. The difference is due, above all, to a higher yield into multibranched isomers (Fig. 4c). The reduction of zeolite crystal size to nanometric scale (40 nm) allowed to increase the maximum yield into isomers (Fig.4 a), but this is not enough since n_{as} is still equal to 1.2.

Scheme 3

Indeed, the formation of large aggregate of nanocrystals favors successive reactions (Scheme 3) [30].

That can be avoided by using nanosponge *BEA-type zeolite, i.e. ultrathin crystals (2-4 nm) separated by structured mesopores. By assuming that the hydrogenolysis reaction did not occur, the 1.4Pt/NS(22) catalyst proved to be totally selective in isomer at high conversion; from a conversion of 75 % multibranched isomers began to crack (Fig. 4). The n_{as} drawn from the initial B/M ratio is 1.08 (Table 4), which means that on this bifunctional catalyst n-hexadecane transformation occurred via a quasi-perfectly successive scheme. The extreme downsizing of the beta crystal is a way to obtain an ideal bifunctional catalyst.

But, the reactional pathway of the 1.4Pt/NS(22) catalyst is not ideal due to the hydrogenolysis reaction

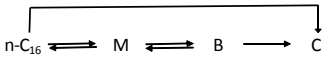

Scheme 4

Nevertheless, a bifunctional catalyst (0.7Pt/(H*BEA/A)) prepared from nano-crystals of *BEA formed by germination on an α-Al_2O_3 surface possess a n_{as} equal to the unity [13] with no hydrogenolysis reaction. In consequence on this real ideal bifunctional catalyst the yield in isomers is higher than on the 1.4Pt/NS(22), and similar in used operating conditions to this obtained with the Pt/HZSM-22, i.e. ca 80 at 90 % conversion (figure SI. 3 [13,31]).

4. Conclusions

n-Hexadecane (n-C_{16}) transformation was studied on a series of bifunctional catalysts with Pt and *BEA-type zeolite as hydro-dehydrogenating and acids components, with large range of crystal size from a dozen of micrometer to few nanometer. Whatever the zeolite crystal size, there is no diffusion limitation during n-C_{16} hydroisomerization. But, before everything else, to design "ideal" bifunctional catalyst acid and metal functions must be "well" balanced. Several simple ways exist to balance a bifunctional such as increasing the amount of metal or decreasing of Si/Al, etc. Regardless of the chosen strategy, the cracking products were always on "well" balanced catalyst secondary products. An "ideal" catalyst, which is characterized by a perfectly successive reaction scheme can be obtained by decreasing the zeolite crystal size to the nanometric scale in order to minimize the residence time of intermediate within the zeolite crystal. But, the extreme downsizing of *BEA crystal to few unit zeolite cells, can cause some unexpected losses of selectivity and activity. The ultrathin zeolite crystal favors metal sintering upon the reduction of the metallic salt in very large particles which are able to hydrogenolyse the n-C_{16}, and the supposed particular spatial distribution of aluminum in ultrathin zeolite could impact the strength of the Brønsted acid sites and in consequence their turnover frequency.

The optimization of platinum deposit and the understanding of the loss of the acid strength in the nanosponge zeolite are two key points to develop an ideal bifunctional catalyst for the hydroisomerization of long-chain paraffins able to compete with the Pt/HZSM-22 catalyst.

Acknowledgment

The authors thank IFPEN for its financial support and the Syrian government for the doctoral grant given to A. Astafan. Ludovic Pinard thank Dr. Fajula agreeing to judge his research work for obtaining His "HDR" in 2012.

References

1 P.B. Weisz,Adv. Catal, 1962 **13**, 137.
2 J. Weitkamp, Chem.Cat.Chem, 2012, **4**, 292.
3 M. Guisnet, Catal. Today, 2013, **123**, 218.
4 C. Bouchy, G. Hastoy, and E. Guillon, J.A. Martens, Oil Gas Sci. Technol. –Rev. IFP, 2009, **64**, 91.
5 A. Soualah, J.L. Lemberton, L. Pinard, M. Chater, P. Magnoux, and K. Moljord, Appl. Catal. A General, 2008, **174**, 1107.
6 J.A. Martens, R. Parton, L. Uytterhoeven, P.A. Jacobs, and G.F. Froment, Appl. Catal, 1991, **76**, 95.
7 J.A. Martens, and P.A. Jacobs, "Zeolite Microporous Solids: Synthesis, Structure and Reactivity, Derouane E.G. et al. Eds, NATO ASI Series C **,** 1992**, 352**, 511.
8 J.A. Martens, W. Souverijns, W. Verrelst, R Parton, G.F. Froment, and P.A. Jacobs, Chem. Int. Ed. Engl 1995**, 34**, 2528.
9 M. Guisnet, J. Mol. Catal 2002, **364**, 182.
10 (M. Guisnet, F. Alvarez, G. Giannetto, and G. Perot, Catal. Today 1987, **1**, 415.
11 F. Alvarez, F.R. Ribeiro, G. Perot, C. Thomazeau, and M. Guisnet, J. Catal, 1996, **162**, 179.
12 N. Batalha, L. Pinard, Y. Pouilloux, and M. Guisnet, Catalysis Letters 2013, **143 (2)**, 587.
13 N. Batalha, L. Pinard, C. Bouchy, E. Guillon, and M. Guisnet, J. Catal, 2013, **307**, 122.
14 K. Na, C. Jo, J. Kim, K. Cho, J. Jung, Y. Seo, R.J. Messinger, B.F. Chmelka, and R. Ryoo, Science 2011, **333**, 328.
15 M. Choi, K. Na, J. Kim, Y. Sakamoto, O. Terasaki, and R. Ryoo, Nature, 2009**, 461**, 246.
16 K. Na, W. Park, Y. Seo, and R. Ryoo, Chem. Mat, 2011, **23** (5), 1273.
17 K. Na, M. Choi, W. Park, Y. Sakamaoto, O Terasaki, and R. Ryoo, J. Am. Chem. Soc, 2010 , **132**, 4169.
18 M.A. Camblor, A. Corma, and S. Valencia, J. Mater. Chem, 1998, **9**, 2137.
19 R.B. Borade, and A. Clearfield, Micro. Mater, 1995, **5**, 289.
20 N. Lauridant, T.J. Daou, G. Arnold, J. Patarin, and D. Faye, Micro. Meso. Mater, 2013, **166**, 79.

21 A. Astafan, M.A. Benghalem, J. Patarin, N. Bats, C. Bouchy, T.J. Daou, and L. Pinard (accepted in J. Catal)
22 C. Coutanceau, J. M. Da Silva, M. F. Alvarez, F. R. Ribeiro, and M. Guisnet, J. Chim. Phys, 1997, **94**, 765.
23 M. Guisnet, P. Ayrault, and J. Datka, Micr. Mes. Mat. 1998, **20**, 283.
24 IUPAC, Pure Appl. Chem, 1985**, 57** (4), 603.
25 A. Simon-Masseron, J.P. Marques, J.M. Lopes, F. R. Ribeiro, I. Gener, M. Guisnet, , Appl. Catal. A. Gen. 207, **316**, 75.
26 A. J.Renouprez, C. Hoang-Van, and P.A. Compagnon, J. Catal., 1974, **34**, 411.
27 E. Verheyen, C. Jo, M. Kuttepeli, G. Vanbutsele, E. Gobechiya, T. I. Koranyi, S. Bala, G. Van Tendeloo, R. Ryoo, E.A. Kirschhock, and J. A. Martens, J. Catal, 2013, **300**, 70.
28 K. Kim, R. Ryoo, H.-D. Jang, and M. Choi, J. Catal., 2012, **288,** 115.
29 J.W. Thybaut, C.S. Laxmi Narasimhan, J.F.M. Benayer, G.V. Baron, P.A. Jacobs, J.A. Martens; G.B. Marin, Ind. Eng. Chem. Res., 2005, **44**, 5159.
30 M. Steijins, G.F. Froment, Ind. Eng. Chem. Res. Dev., 1981, **20**, 654.
31 N. Batalha, S. Morisset, L. Pinard, I. Maupin, J.L. Lemberton, J.L. F. Lemos, and Y. Pouilloux, Micro Meso. Mat ,2013, **166**, 161.
32 N. Batalha, L. Pinard, S. Morisset, J.L. Lemberton, Y. Pouilloux, M. Guisnet, F. Lemos, and F. R. Ribeiro, React. Kin. Mech. Catal. 2012**, 107**, 285.

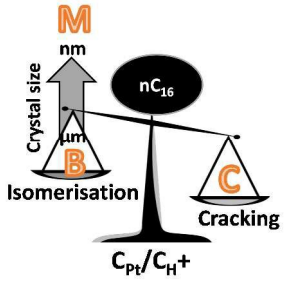

The extreme diminution of crystallite size increases accessibility of Brønsted acid sites but decreases their strength.